Variability of the mixed layer heat budget in the eastern equatorial Atlantic during 2005-2007 as inferred using Argo floats

M. Wade, G. Caniaux, Y. Du Penhoat

Variability of the mixed layer heat budget in the eastern equatorial Atlantic during 2005–2007 as inferred using Argo floats

Malick Wade,[1,2,3,4] Guy Caniaux,[2] and Yves du Penhoat[1,3]

Received 29 September 2010; revised 4 May 2011; accepted 12 May 2011; published 10 August 2011.

[1] We examine the variability of the sea surface temperatures in the eastern equatorial Atlantic during 2005–2007 by using Argo profiling floats, Prediction and Research Moored Array in the Atlantic buoys and satellite, in situ, and atmospheric data sets. The eastern equatorial Atlantic, characterized by shallow mixed layers all yearlong, is divided into nine boxes of nearly equal surface area, with respect to the dynamics and thermodynamics in this region. Monthly mixed layer heat budgets are computed in each box from 10 day Argo profiles. In all the boxes, the net surface heat flux is one of the main causes of the seasonal evolution of sea surface temperatures for the 3 studied years. The amount of short-wave radiation penetrating through the base of the mixed layer and horizontal heat advection may locally contribute to the temperature variability, while entrainment has a weaker contribution. To balance the heat budget, a residual term exists which includes all processes that cannot be calculated with observations as well as the possible errors in the other terms. This residual is more intense in the cold tongue and the northern region and exhibits a clear seasonal cycle, with minimum (negative) values in boreal summer and maximum values in winter. This residual compares well with available observations of vertical turbulent mixing collected during Etude de la Circulation Océanique et des Échanges Océan-Atmosphère dans le Golfe de Guinee campaigns (2005–2007) in the eastern equatorial Atlantic. When assuming that the residual is mostly associated with vertical turbulent mixing, it can be conjectured that turbulent mixing is a significant cooling source in the cold tongue and north of the equator.

Citation: Wade, M., G. Caniaux, and Y. du Penhoat (2011), Variability of the mixed layer heat budget in the eastern equatorial Atlantic during 2005–2007 as inferred using Argo floats, *J. Geophys. Res.*, *116*, C08006, doi:10.1029/2010JC006683.

1. Introduction

[2] The eastern equatorial Atlantic (15°W, 15°E and 10°S, 6°N) (EEA) is the place where the Atlantic Cold Tongue (ACT) appears. In the ACT, sea surface temperatures (SSTs) drop relatively fast in spring and early boreal summer, by as much as 7°C [*Merle*, 1980; *Picaut*, 1983]. The ACT extends from the African coast to roughly 20°W and reaches its minimum temperature near 10°W at the equator and then propagates to the west [*Carton and Zhou*, 1997].

[3] The source of year-to-year variability of SSTs in the EEA is not well known. For example, the years 2005 and 2006 exhibited contrasting SST evolution in the EEA in boreal summer. In 2005, the cooling started earlier than usual (mid-May), while in 2006 SSTs were warmer and a time shift (1 month) in the ACT appearance was observed [*Janicot et al.*, 2008; *Marin et al.*, 2009]. The 2006 minus 2005 SSTs in the ACT region were up to 3°C. *Marin et al.* [2009] attributed the unusually cool SSTs in 2005 to both the basin preconditioning and earlier, more intense south-easterly winds in the western tropical Atlantic south of the equator.

[4] Recently, using statistical analyses based on *Reynolds et al.*'s [2007] SST data set, *Caniaux et al.* [2011] found that, during the past 3 decades, the lowest SST values in the ACT were reached in 1982 and 2005. They found a year-to-year variability of (1) the spatial extension of the ACT, (2) its dates of formation, and (3) its duration. The authors also found a high correlation between the dates of the ACT formation and the African monsoon jump (up to 80%), in agreement with *Brandt et al.* [2011] who determined lagged regression patterns of SST, wind, and rainfall associated with variable ACT and monsoon onset dates.

[5] Using statistical analyses based on TMI SSTs and QuickSCAT surface wind measurements, *de Coëtlogon et al.* [2010] investigated the intraseasonal variability of air-sea interactions in the Gulf of Guinea (GG) during spring and summer. They found the existence of wind peaks around 15 days and a maximum correlation between SSTs and winds with a 5 day lag with the wind forcing, suggesting that there is strong coupling between SSTs and the surface winds in the GG.

[1]LEGOS, IRD, Toulouse, France.
[2]CNRM/GAME, Météo-France/CNRS, Toulouse, France.
[3]LEGOS, Université de Toulouse, OMP, UPS, Toulouse, France.
[4]Now at LPAOSF, UCAD, Dakar, Senegal.

0148-0227/11/2010JC006683

[6] Based on the findings cited above, it is necessary to examine the seasonal SST variability in the EEA closely. A number of observational [*Merle*, 1980; *Foltz et al.*, 2003] and modeling studies [*Philander and Pacanowski*, 1986; *Yu et al.*, 2006; *Peter et al.*, 2006] have addressed the causes of the seasonal cycle of SSTs in the EEA. They indicate that, in the ACT, the main cooling is due to vertical subsurface processes (vertical advection, mixing and entrainment), which are nearly balanced by the warming due to atmospheric fluxes, but horizontal advection can also make a significant contribution locally. Off equator, *Foltz et al.* [2003] found that the balance is mainly one-dimensional and highly dominated by latent heat fluxes. The authors also found strong time-space SST variability associated with the surface current, the subsurface processes and the net surface heat fluxes.

[7] In the EEA, the availability of hydrographic observations has increased strongly in recent years due to enhanced shipboard observations and the increased number of Argo floats deployed in this region. In the GG, several research cruises were carried out in the framework of the French Etude de la Circulation Océanique et des Échanges Océan-Atmosphère dans le Golfe de Guinee (EGEE) program [*Bourlès et al.*, 2007] as part of the AMMA program (http://www.amma-international.org/) [*Redelsperger et al.*, 2006]. To assess seasonal and interannual variability, six EGEE cruises were conducted, with two cruises per year during 2005–2007. Cruises were scheduled to coincide with the monsoon onset and the development of equatorial upwelling in early boreal summer (end of May to July), and during the mature phase of the monsoon (September–October) when the ACT is still well developed.

[8] Thanks to the EGEE cruises, the number of subsurface observations in the eastern equatorial and tropical south Atlantic strongly increased also in the recent years mainly due to an increased number of Argo floats deployed in this region. These data complement with the Prediction and Research Moored Array in the Atlantic (PIRATA) network [*Bourlès et al.*, 2008] which provides high-resolution time series of surface heat and water fluxes, SST and sea surface salinity (SSS), and subsurface temperature and salinity in the upper 500 m at fixed points.

[9] Argo profiling floats have been used already in different broad regions, either to study the mixed layers in the northern Pacific [*Ohno et al.*, 2004] or to estimate the mixed layer heat budget in the northern Atlantic [*Hadfield et al.*, 2007; *Wells et al.*, 2009; *de Boisséson et al.*, 2010]. Some authors obtained a good estimate of the mixed layer heat budget and concluding that the accuracy of Argo profiling was reliable. However, to our knowledge, any studies on the mixed layer heat budget using Argo have yet concerned the equatorial regions, especially the EEA. Other estimates of the main terms of the heat budget have been obtained from different types of data but with large residuals [*Swenson and Hansen*, 1999; *Wang and McPhaden*, 1999; *Foltz et al.*, 2003].

[10] Here, we use the Argo profiling floats combined with four PIRATA buoys to study the mixed layer heat budget in the EEA during 2005–2007, a period in which a consistent time series of temperature/salinity profiles could be retrieved to assess the seasonal and interannual variability of SSTs. The aim of this paper is not to close the budget since it is a very hard task with observational data only. Our objective is to provide new estimates of the causes of SST seasonal variability in the EEA with an original data set as the main source of data. It is also the opportunity to check whether the Argo profiling floats are suitable to give accurate estimates of the mixed layer heat budget in the EEA. Compared with *Foltz et al.* [2003], our study aims also at providing a better regionalization of the heat budget over the EEA and to provide a better estimate than at fixed points.

[11] The remainder of this paper is organized as follows. Section 2 describes the Argo and PIRATA data and the data processing procedure, followed by a description of the additional surface data necessary to compute the budget. In section 3, the mixed layer heat budget computation used in this study is presented. Section 4 describes mean, seasonal, and interannual variations of the budget in the region. The paper concludes in section 5 with summary and discussion of the most important results.

2. Data

2.1. Argo Data Set

[12] The Argo float project [*Roemmich et al.*, 2001; *Gould*, 2005] provides high-quality subsurface temperature and salinity data. Currently, more than 3000 floats are sampling the ocean. The floats are deployed by 23 countries with the most important contribution by the U.S. APEX, SOLO, and PROVOR are the most widely used profilers, contributing 61%, 26%, and 11%, respectively, to the total number of Argo floats used since 1999. Floats are launched from research vessels, container ships and aircraft. When deployed from a ship, the float is dropped into the ocean and starts profiling on its ascent to the surface from a depth of 2000 m. Buoyancy is controlled by a pressure regulating mechanism that varies the volume of oil in a chamber in the float. The total cycling time is approximately 10 days. A cycle involves an initial descent to a drifting depth of 1000 m, drifting at 1000 m for approximately 9 days, descent to 2000 m and an ascent stage (approximately 10 h), where temperatures and salinities are recorded at regular intervals. When it surfaces, the float transmits all stored data to space satellites, which relay data to earth stations. The float then dives to begin a new cycle. The Argo data are available at the Coriolis data center (http://www.ifremer.fr/coriolis/) and are quality controlled in real time and, for some of them, in delayed mode. The nominal accuracy on temperature and salinity is 0.01°C and 0.01, respectively.

[13] In the EEA, 68 floats drifted from 2005 to 2007 and 3409 profiles were retrieved. The Argo data used in this study includes both data in real-time and delayed mode. Whereas any drift, or offset, of the pressure sensors is internally corrected in PROVOR and SOLO floats, in the case of APEX floats, it is usually carried out at the Argo Data Assembly Center. As this correction was not available in our data set, following Argo recommendations, we applied our own Quality Control (QC) and checked that none of the floats under consideration in this study were concerned by the microleak known to affect some of the Druck pressure sensors [*Riser*, 2009]. Our QC check allowed also individual inspections of profiles in order to

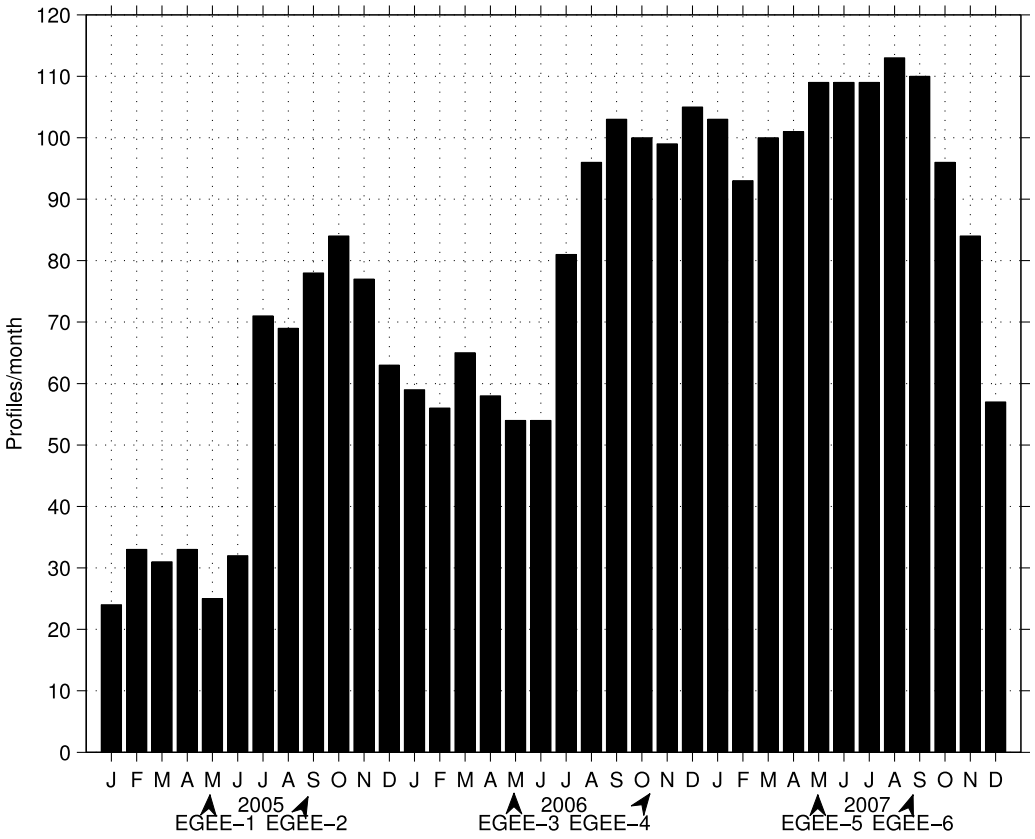

Figure 1. Monthly number of Argo profiles in the domain of study (15°W, 15°E and 10°S, 6°N). The EGEE campaigns (May–June–September in 2005, 2006, and 2007) are indicated with arrows.

obtain high-quality data even in the top surface layers. The correction removed 7% of the Argo profiles. The QC method that we developed is presented in Appendix A.

[14] Figure 1 gives the histogram of the monthly mean profiles during 2005–2007. It shows that 2005 was less sampled than 2006 and 2007. The number of profiles has considerably increased since 2005. Starting from 20 profiles per month in January 2005, it reached 100 profiles per month in January 2007. Moreover, profiles are mainly clustered after May–June, which reflects the increasing number of floats deployed during the AMMA/EGEE campaigns in the EEA.

2.2. PIRATA Data Set

[15] To complement Argo data, PIRATA data sets were also used to fill temporal and spatial gaps in the Argo profiles. The PIRATA mooring array [*Bourlès et al.*, 2008] is an in situ observation array of moored buoys designed to monitor a set of atmospheric and oceanographic variables of the ocean-atmosphere interface processes in the tropical Atlantic Ocean. The array currently consists of 17 buoys and we focus on four of them located in the EEA. Deployed since 1997 to study ocean-atmosphere interactions, these Next Generation Autonomous Temperature Line Acquisition System (ATLAS) buoys measure temperatures at 11 recorded depths between 1 and 500 m with 20 m spacing in the upper 140 m, while salinity (via conductivity) is measured at four depths: 1, 20, 40, and 120 m. In this study, data from 3 PIRATA moorings are used (along 10°W and at 0°, 0°). The QC developed for Argo floats was also applied to the PIRATA data. The QC procedure excluded 5% of the overall PIRATA data (550) from our analysis (data are available at: http://www.pmel.noaa.gov/pirata/).

2.3. Surface Heat Fluxes and Additional Data Sets

[16] Computing the mixed layer heat budget also needs surface heat fluxes, currents, and SSTs for the horizontal advection calculation. For this purpose, the European Center for Medium-Range Weather Forecasts (ECMWF) data set was chosen for the surface heat fluxes, the Ocean Surface Current Analyses – Real Time (OSCAR) [*Bonjean and Lagerloef*, 2002] data was used for the ocean horizontal current and the data by *Reynolds et al.* [2007] provided daily SSTs.

[17] ECMWF surface heat fluxes were selected because, of the NWP models, they validated best against in situ data collected during the EGEE-3 campaign in 2006 [*Caniaux et al.*, 2007; *Brandt et al.*, 2011]. The ECMWF surface flux data contain net short- and long-wave fluxes and sensible and latent heat fluxes. This data set was provided on a grid with regular horizontal spacing of 0.5° longitude and 0.5° latitude. The fluxes were linearly interpolated into a 0.25° × 0.25° grid, compatible with the grid of *Reynolds et al.*'s [2007] daily SSTs.

[18] The OSCAR horizontal velocity is a combination of geostrophic and Ekman currents, is representative of flow in the mixed layer at 15 m depth and is available on a 1° × 1° grid. The data is available at the OSCAR Web site (http://

www.oscar.noaa.gov/). The method for calculating ocean near surface currents is fully discussed by *Bonjean and Lagerloef* [2002] and here we just outline the basis of the method.

[19] OSCAR currents are calculated at 5 day intervals, with each 5 day map being derived from a previous map of Sea Surface Height (SSH) calculated from different available satellite altimeters, scatterometer winds, and in situ SSTs representing the surrounding ~10 days of data [*Johnson et al.*, 2007], which result in an effective resolution of 10 days.

[20] The method is based on the resolution of quasi-linear and quasi-steady momentum equations [*Bonjean and Lagerloef*, 2002]. Caution is exercised near the equator where the Coriolis parameter vanishes. Further details of this data set are given by *Bonjean and Lagerloef* [2002], *Helber et al.* [2007], and *Johnson et al.* [2007] for validation and error analyses. These data are also linearly interpolated on the same 0.25° × 0.25° grid and daily means are used to estimate the horizontal advection.

3. Heat Budget Method

[21] The heat budget in the mixed layer can be expressed as [see, e.g., *Caniaux and Planton*, 1998]

$$\rho_0 C_p h \partial_t \langle T\rangle = \rho_0 C_p \left[-h\langle U\rangle.\nabla\langle T\rangle - \nabla \int_{-h}^{0} \tilde{U}\tilde{T}dz - [\langle T\rangle - T(-h)]w_e(-h) + \overline{w'T'}(-h) + hA_H\nabla^2\langle T\rangle \right] + F_{net} + Q_{pen}, \quad (1)$$

with

$$F_{net} = F_{sol} + F_{nsol}. \quad (2)$$

T is the potential temperature of the float; U is the horizontal velocity with (u, v) the eastward and northward components of the velocity; w is the vertical velocity; h the mixed layer depth (MLD) and A_H the horizontal eddy diffusivity; and C_p and ρ_0 are the specific heat capacity per unit volume and the surface-referenced density, respectively (with ρ_0 set to 1024 kg m^{-3} and C_p to 3984 J kg^{-1} °C^{-1}). F_{net} is the net surface heat flux, F_{sol} the short-wave radiation and F_{nsol} the sum of the sensible heat, latent heat fluxes and net long-wave radiation.

[22] $\nabla \equiv (\partial/\partial x, \partial/\partial y)$ is the horizontal gradient operator; x, y, and z are the eastward, northward, and upward coordinates, respectively; and t is the time. We define the vertical average of any variable a over the mixed layer as $\langle a\rangle = \frac{1}{h}\int_{-h}^{0} a dz$ and we note $\tilde{a} = a - \langle a\rangle$ the deviation from this average. $w_e(-h)$ is the entrainment velocity, defined as

$$w_e(-h) = w(-h) + \partial_t h + U(-h)\nabla h. \quad (3)$$

[23] The individual terms of equation (1) represent, from left to right: the heat storage, the horizontal advection of heat, the temperature and horizontal velocity covariance, the entrainment-induced heat at the mixed layer base, the vertical turbulent mixing at the mixed layer base, the horizontal heat diffusion, the net surface heat fluxes and the amount of short-wave radiation passing through the base of the mixed layer (Q_{pen}). All surface fluxes are positive when they represent gains to the mixed layer. We estimate the MLD (h) by using a temperature criterion as *de Boyer Montégut et al.* [2004]. The MLD is defined as the depth at which the temperature differs by less than 0.2°C from its surface value. In the entrainment term (equation 3), the vertical velocity at the mixed layer base is estimated from the continuity equation

$$w(-h) = \int_{-h}^{0} \left[\frac{\partial u}{\partial x} + \frac{\partial v}{\partial y}\right] dz. \quad (4)$$

[24] It was further assumed that the horizontal divergence is depth independent in the mixed layer so that the equation of continuity reduces to

$$w(-h) = h\left[\frac{\partial u}{\partial x} + \frac{\partial v}{\partial y}\right]. \quad (5)$$

Here u and v are taken from OSCAR currents. As in equation (3) ∇h cannot be estimated from individual profiles, we use the MLD climatology based on Argo and other available data (moorings, XBT and CTD) produced by the Coriolis data center (available on request) to estimate ∇h. The MLD climatology is interpolated at a daily resolution for use in equation (3).

[25] The parameterization of *Ohlmann* [2003] and *Sweeney et al.* [2005] is used to estimate Q_{pen}, i.e.,

$$Q_{pen} = 0.47F_{sol}(V_1 e^{-h/d_1} + V_2 e^{-h/d_2}), \quad (6)$$

where d_1 and d_2 are the e-folding depths of the long visible (d_1) and short visible and ultraviolet (d_2) wavelengths. The parameters V_1, V_2, d_1, and d_2 are estimated using the monthly mean seasonal cycle of SeaWiFS chl-a concentration interpolated at a daily frequency, following *Sweeney et al.* [2005] (the SeaWiFS data were downloaded from the Web site http://oceancolor.gsfc.nasa.gov/SeaWiFS/).

[26] As we assume that the temperature is uniform from the surface to the mixed layer base, then SST is taken as $\langle T\rangle$ when computing the horizontal advection term in equation (1). Daily *Reynolds et al.*'s [2007] SSTs are then used to estimate $\nabla\langle T\rangle$ in equation (1). In the same way, $\langle U\rangle$ is supposed to be uniform on the vertical and is taken from OSCAR current data (U). Moreover, the assumption that the temperature is uniform in the mixed layer results also in the neglect of the temperature and horizontal velocity covariance term ($\nabla \int_{-h}^{0} \tilde{U}\tilde{T}dz$) in equation (1), a small term compared to other terms [*Swenson and Hansen*, 1999].

[27] Because of the lack of knowledge of magnitude and spatial variations of vertical mixing coefficients, several authors [e.g., *Wells et al.*, 2009] estimated the vertical turbulent mixing term by assuming a constant mixing coefficient in their mixed layer budget computations. This procedure is subject to high uncertainties, especially in the ACT area where the coefficients are thought to be large and have a strong dependence on seasonal atmospheric and

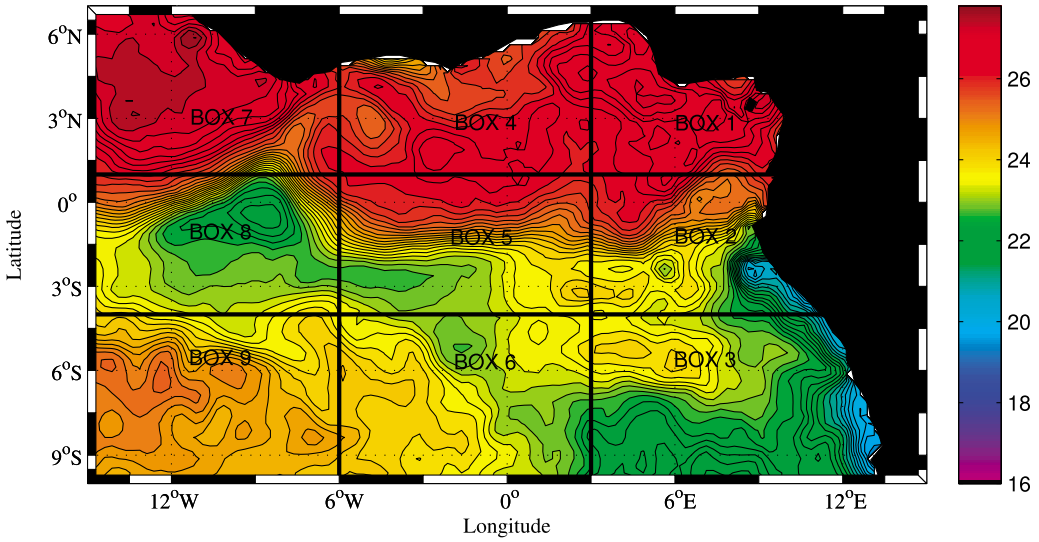

Figure 2. Spatial delimitation of the nine boxes in the eastern equatorial Atlantic. SSTs from *Reynolds et al.* [2007] at 15 July 2005 are plotted.

oceanic changes as proved by in situ data [e.g., *Gouriou and Reverdin*, 1992; *Rhein et al.*, 2010] or modeling studies [*Foltz et al.*, 2004; *Menkes et al.*, 2006; *Jochum and Murtugudde*, 2006]. This is why we preferred to include this term into the residual in this study. We supposed that the horizontal heat diffusion is small and has been neglected thereafter. This term is nonnegligible only locally in region of large temperature heterogeneity, but here neglecting this term is a reasonable hypothesis as calculations are carried out over sufficiently large areas [*Caniaux and Planton*, 1998]. Finally, the mixed layer heat budget equation that was computed from Argo and PIRATA data can now be expressed as follows:

$$\rho_0 C_p h \partial_t \langle T \rangle = \rho_0 C_p [-hU.\nabla SST - [\langle T \rangle - T(-h)]w_e] + F_{net} + Q_{pen} + RES, \quad (7)$$

where w_e is given by equation (3) and *RES* stands for the residual which represents the combination of errors and terms that cannot be directly estimated from our data.

[28] Taking previous studies into consideration [e.g., *Merle*, 1980; *Foltz et al.*, 2003; *Peter et al.*, 2006], the EEA is divided into nine boxes of roughly equal surface area (Figure 2) that reflect the regional heterogeneities of the dynamics and thermodynamics of the EEA on seasonal time scales. The latitudinal bands are defined as follows:

[29] 1. The northern boxes (boxes 1, 4, and 7) are located north of the equatorial SST front (nearly 1°N) separating the warm SSTs at north from the equatorial cooler waters at south. These boxes are also under the influence of the Guinea Current, which exhibits its minimum speed during winter and a maximum during summer [*Bakun*, 1978; *Richardson and Philander*, 1987; *Colin*, 1988].

[30] 2. ACT boxes (boxes 2, 5, and 8) correspond to the ACT region (from 1°N to 4°S). This region is under the influence of the surface South Equatorial Current (SEC) and the Equatorial Undercurrent (EUC) [*Stramma and Schott*, 1999], the summer shoaling of which directly impacts the SST variability through intense mixing with the SEC [*Hormann and Brandt*, 2007]. The net surface heat flux in this band is positive all yearlong, balancing the SST cooling by subsurface processes [*Yu et al.*, 2006].

[31] 3. In the southern band from 10°S to 4°S (boxes 3, 6, 9), the SST variability is mainly driven by the surface heat fluxes [*Foltz et al.*, 2003; *Yu et al.*, 2006; *Peter et al.*, 2006] and subsurface processes are expected to be weak except in box 3, which is under the influence of coastal upwelling.

[32] The longitudinal bands are defined as follows:

[33] 1. The boxes 1, 2 and 3 represent the coastal band under the influence of the African continent. In this band (from the coast to 3°E), MLDs are weaker than elsewhere all yearlong and vary from 5 to 20 m [*Vauclair and du Penhoat*, 2001].

[34] 2. The band between 6°W and 3°E (boxes 4, 5, 6) defines the central part of the GG.

[35] 3. The western band from 15°W to 6°W (boxes 7 and 8), is the region were the tropical instability waves (TIW) develop and migrate westward, while box 9 is under the influence of the southern Atlantic.

[36] Figure 3 represents the time-latitude distribution of Argo and PIRATA profiles in each box and the number of profiles in each box is reported in Table 1. Profiles are more numerous in the western side of the domain, due both to the area of deployment and to the mean circulation.

[37] In the mixed layer computation, budgets are primarily computed from individual floats (i.e., along float trajectories) by using a finite centered difference scheme between two consecutive profiles separated by the time step *dt*, the total cycling time of the Argo floats. During this time step (10 days), advection, entrainment, the net surface heat fluxes and the amount of short-wave radiation penetrating through the base of the mixed layer in equation (7) are evaluated every day at the Argo position (obtained by linear interpolation of the 10 day position of the float), and then averaged over the time step. The same procedure is applied to PIRATA profiles (except that they are at fixed positions).

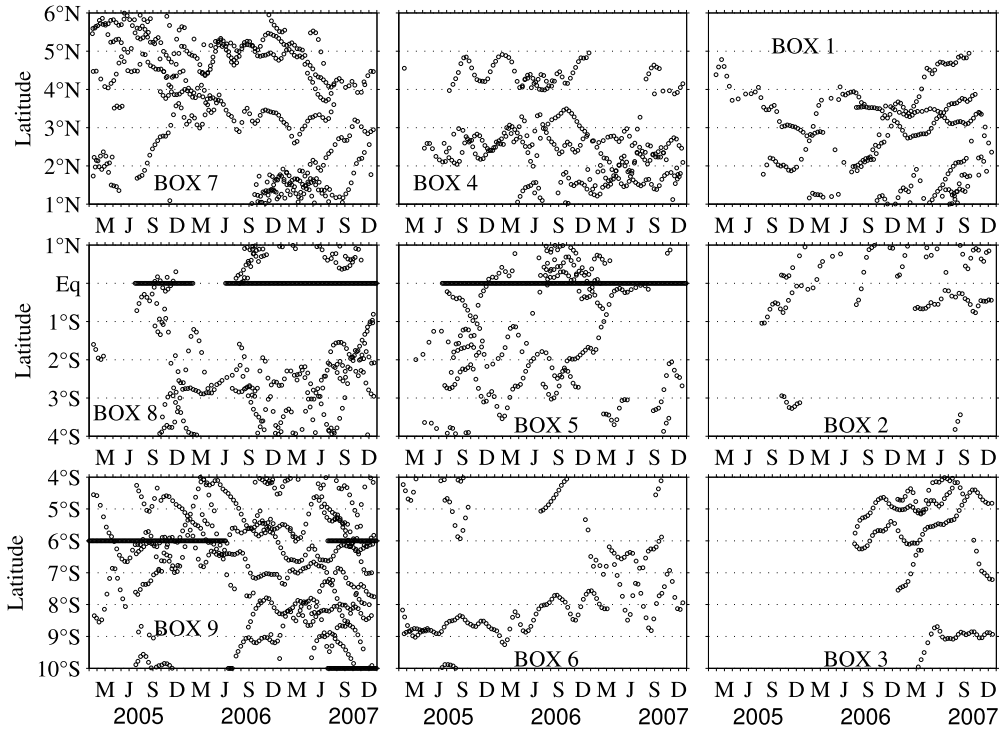

Figure 3. Latitude-time diagram of the number of Argo and PIRATA (black lines) profiles in each box.

[38] However *dt* is not always equal to 10 days due to the removal of some profiles by our QC. A condition in the mixed layer heat budget computation is then imposed: if the time period between two consecutive profiles is greater than 1 month, the budget is not estimated because this period is thought to be too great to give representative budgets. Finally, mixed layer heat budgets from Argo and PIRATA have been averaged to obtain monthly values in each box.

4. Results

4.1. SST Interannual Variability: Comparison With Reynolds' SSTs

[39] The monthly mean variations of SSTs, as inferred from Argo floats, are shown in Figure 4, where they are compared with monthly averaged SSTs [*Reynolds et al.*, 2007]. The comparison shows a good agreement in terms of phasing and amplitudes. Correlations between the two independent data sets exceed 89% in all boxes and the RMS differences are less than 0.3°C. This agreement also gives confidence in our QC. The time variation of SSTs (Figure 4) shows a clear annual cycle, with a warming observed from September to March with maxima in March. From March, they decrease gradually to a minimum in July–August. The maxima of SST amplitudes occurs in boxes 3 and 5 (up to 6°C; Table 1), where the coastal upwelling and the ACT connect in summer. As expected, a strong north-south SST gradient up to 3°C (Figure 4) is clearly visible between the ACT boxes and the northern boxes. These north-south gradients have a direct link with the African monsoon intensity [*Lamb*, 1978; *Gu and Adler*, 2004; *Caniaux et al.*, 2011]. The low-level atmospheric convergence that develops in these areas feeds the Intertropical Convergence Zone (ITCZ).

Table 1. Characteristics in the Different Boxes[a]

	Number of Profiles	Temperature (°C)			Summer Residual (Wm^{-2})	K_v ($cm^2\ s^{-1}$)	K_v [*Rhein et al.*, 2010] ($cm^2\ s^{-1}$)	K_v During FOCAL [*Gouriou and Reverdin*, 1992] ($cm^2\ s^{-1}$)
		Minimum	Maximum	Amplitude				
Box 1	275	26.0	29.5	3.5	−20	0.3	–	–
Box 2	124	24.0	29.5	5.5	−9	0.3	–	–
Box 3	143	22.8	28.8	6.0	−65	1	–	–
Box 4	334	25.0	30.0	5.0	−70	3	–	–
Box 5	444	23.0	29.0	6.0	−53	1	1	2
Box 6	167	22.2	28.0	5.8	−17	0.9	–	–
Box 7	496	26.0	29.5	3.5	−52	1.5	–	–
Box 8	453	23.0	28.5	5.5	−75	2	1.5	3
Box 9	750	23.8	28.5	4.7	−15	0.9	–	–

[a]The number of selected Argo profiles after the QC check; minimum, maximum, and amplitude of the SST seasonal cycle in each box; residual of the heat budget computed for the summer months (June–July–August); and the corresponding vertical mixing coefficient estimated from the summer residual are shown. Mixing coefficients estimated by *Rhein et al.* [2010] and *Gouriou and Reverdin* [1992] are also shown for comparison.

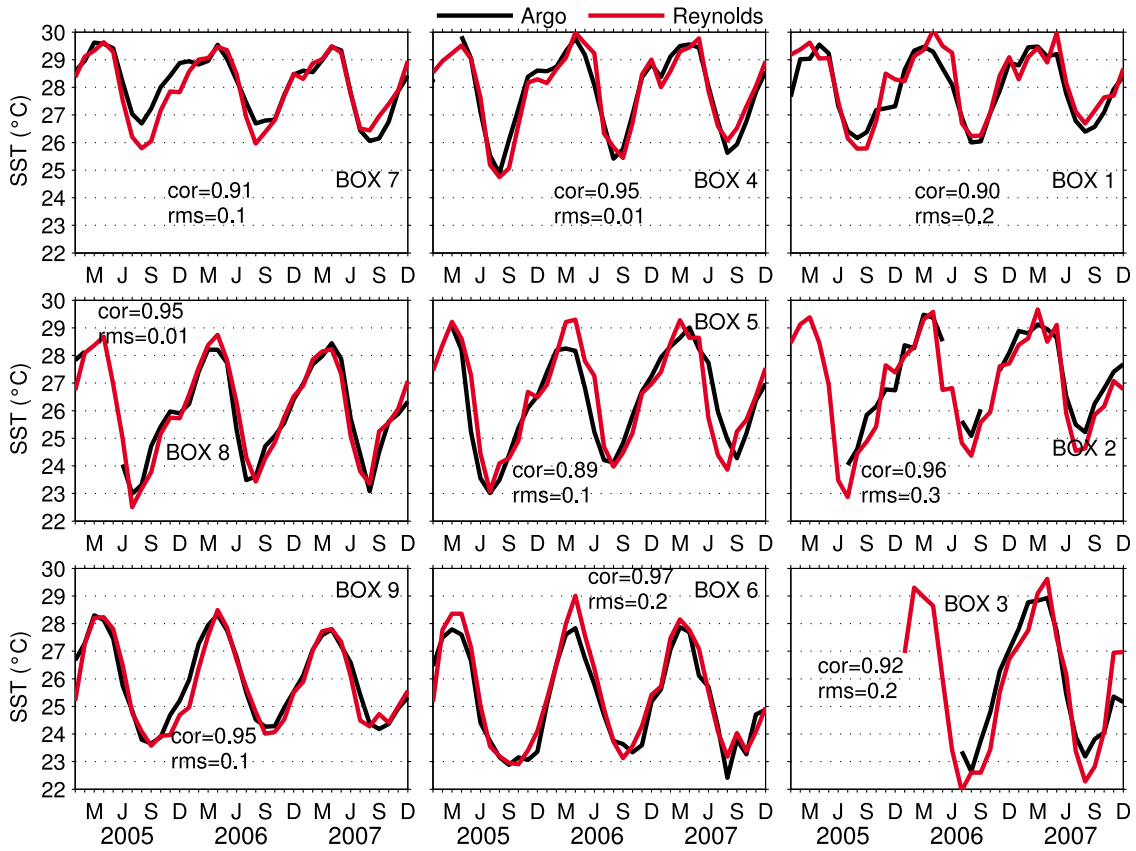

Figure 4. Interannual variability of the monthly sea surface temperature (°C) in 2005–2007 in the different boxes from Argo data (black) and from *Reynolds et al.* [2007] (red). Correlations and root-mean-square differences are also indicated.

4.2. Time Evolution of the Upper Layer Structure During 2005–2007

[40] In hydrographic profiles collected in 2005 and 2006 during EGEE cruises, the upper ocean structures along 10°W showed equatorward shoaling of the thermocline (i.e., the depth of 20°C isotherm (D20), which is a proxy of the thermocline) and the MLD in both years, with depths in 2006 twice that of 2005 [*Marin et al.*, 2009]. The cruises also revealed that, near the equator, the D20 and the MLD were observed at 30 and 10 m, respectively, between 3°S and 1°N in 2005, whereas they were both 20 m deeper in 2006 [*Marin et al.*, 2009]. It was also observed that the ACT was set up prematurely in 2005 (starting in mid-May and lasting at least 4 months) compared to 2006, making 2005 the year of earliest ACT onset over the last 27 years [*Caniaux et al.*, 2011]. The 2005 ACT was thus observed to stay 3°C colder than in 2006 from mid-May to mid-July. The authors attributed these unusually cool SSTs found in 2005 to both the basin preconditioning and to earlier, intense southeasterly winds as already said in the introduction.

[41] The results of these papers are consistent with the data provided by the Argo as can be seen in Figures 4 and 5 for the SSTs and temperature profiles, respectively, in the upper 100 m. Contrasted SSTs in early boreal summer between 2005 and 2006 and between 2005 and 2007 are detected in the ACT boxes (5 and 8) (Figure 4). Cooling in the mixed layer was more intense in 2005 than in 2006 and 2007, both in the ACT (box 8) and in the southern part of the domain (box 9). These differences did not exist in the northern boxes (see for instance box 7 in Figure 5). MLDs and D20 exhibit significant differences only in the ACT region (box 8).

4.3. Heat Budget

4.3.1. The 2005–2007 Mean

[42] Box-to-box annual means of heat storage (Figure 6) are positive everywhere (maximum 22 W m^{-2} in box 8) except in boxes 6, 7, and 9 where they are negative (minimum –11 W m^{-2} in box 9), meaning that at a 3 year scale, the heat storage term can exhibit a weak cooling or warming tendency. Note that the 3 years 2005–2007 were very contrasted in term of SST evolutions in the GG [*Janicot et al.*, 2008; *Marin et al.*, 2009].

[43] Examination of the annual means shows that the most important term of the budget is the net surface heat flux, in agreement with previous studies [*Merle*, 1980; *Foltz et al.*, 2003; *Peter et al.*, 2006]. The ratio of the net surface heat flux (taken as its absolute value divided by the sum of all the absolute values of the terms on the right-hand side (rhs) of equation (7)) explains 40–50% of the annual budget and is maximum (values greater than +89 W m^{-2}) in the ACT (boxes 5 and 8) and in the eastern coastal band (boxes 1, 2, and 3). Moreover, the annual net surface heat flux is positive everywhere with minimum values (less than +40 W m^{-2}) in

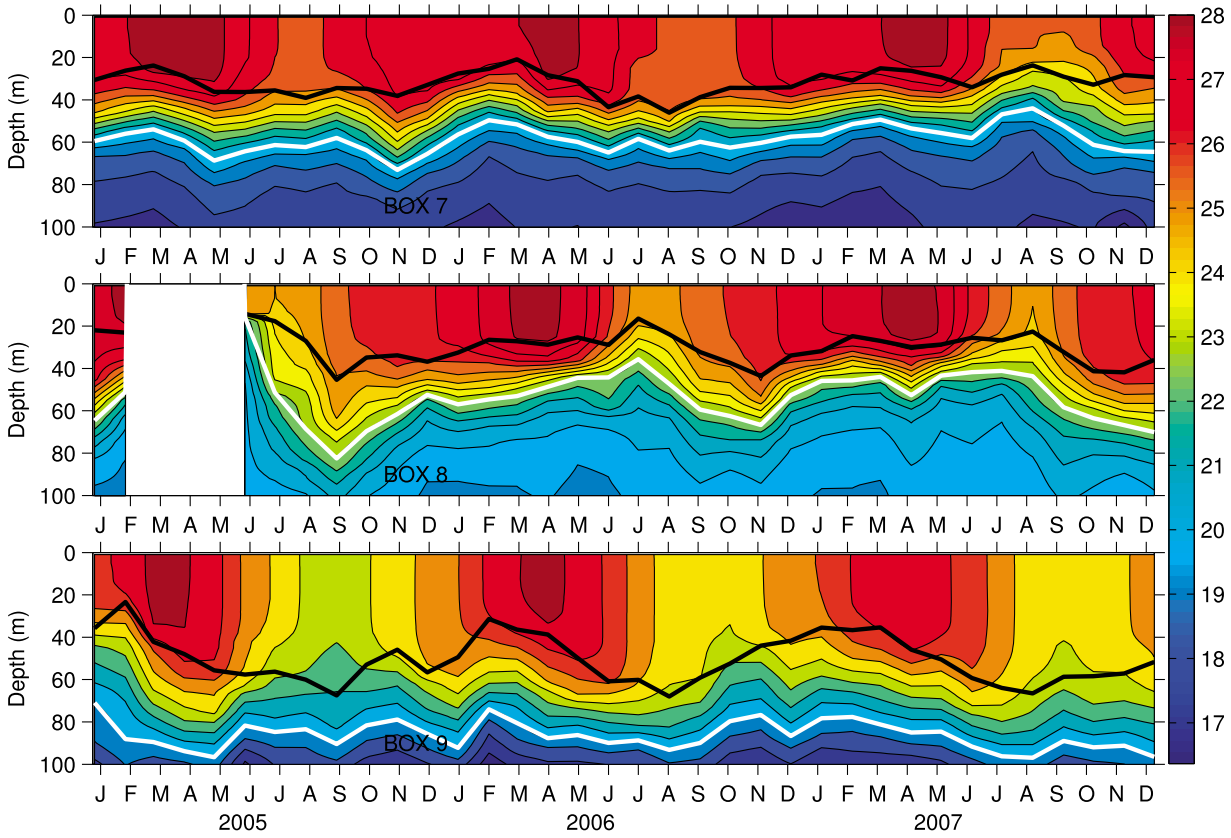

Figure 5. Time-depth sections of the temperature profiles (°C) for boxes (top) 7, (middle) 8, and (bottom) 9. The mixed layer depth (computed as the average of individual profile mixed layer depths) is indicated in black and the depth of the 20°C isotherm in white.

the southern boxes (6 and 9), where the strong evaporation cooling dominates the net solar radiation warming.

[44] The amount of solar radiation passing through the mixed layer base (Q_{pen}) has a net annual mean ranging between –13 and –40 W m^{-2}, which represents a significant part of the budget (10–26%). Maximum cooling due to this term is found in areas where MLDs are on average the weakest, i.e., in boxes near the eastern African coast (boxes 1, 2, and 3). The annual mean of heat advection is negative in all the southeastern boxes (1, 2, 3, 5, 6, and 9), while in the remaining northwestern boxes this term makes a positive contribution to the budget. However, the contribution of horizontal advection is significant only in boxes 1, 2, 8, and 9, where it represents 9%, 13%, 8%, and 28%, respectively, of the budget. Entrainment is negative in all boxes with a contribution less than 10% of the heat budget and generates maximum cooling in the ACT boxes (−11 and −13 W m^{-2} in boxes 5 and 8, respectively). Substantial residuals are found in all boxes, always with negative values, and contribute to more cooling (−25 to −53 W m^{-2}) in the northern boxes (1, 4, and 7) and in the ACT (boxes 5 and 8) than in the southern boxes, especially in box 9 (−3 W m^{-2}).

[45] The sign of each term of the budget is in agreement with the results of *Foltz et al.* [2003] but their magnitudes are somewhat weaker in our study. The differences are probably due to the different considered regions and also to the formalism used to compute the mixed layer heat budget. *Foltz et al.* [2003] used PIRATA buoys, which represent single points in the Atlantic, while in our study, the budgets are computed in large boxes, where spatial averaging may contribute to smooth results. The differences can also be due to the length of the time series used to compute the budget: *Foltz et al.* [2003] used 6 years (1997–2002) PIRATA data while, in the present study, only 3 years (2005–2007) are considered.

4.3.2. Seasonal Variability

[46] At seasonal time scales, the range of heat storage term is between –100 and +75 W m^{-2} (Figure 7). Moreover, Figure 7 shows strong temporal and spatial heterogeneity (1) in box-to-box amplitude of cooling/warming, (2) at the beginning of the cooling, and (3) in cooling duration.

[47] In all boxes, the cooling starts in April and its maximum is observed in June–July, except in box 5 where cooling starts earlier (March) and the maximum is also reached earlier (May). The cooling is associated with the seasonal strengthening of the trade winds in the equatorial Atlantic. Note the occurrence of a delay between the maximum cooling in box 8 (June) compared to box 2 (May). On the other hand, warming is observed from September to April and weakens in November–December in the northern and ACT boxes, a period known as the "short cold season," the magnitude of which is small compared to the boreal summer ACT.

[48] These findings are in agreement with previous mixed layer heat budget studies in the equatorial Atlantic [e.g., *Merle*, 1980; *Peter et al.*, 2006]. Furthermore, our results in

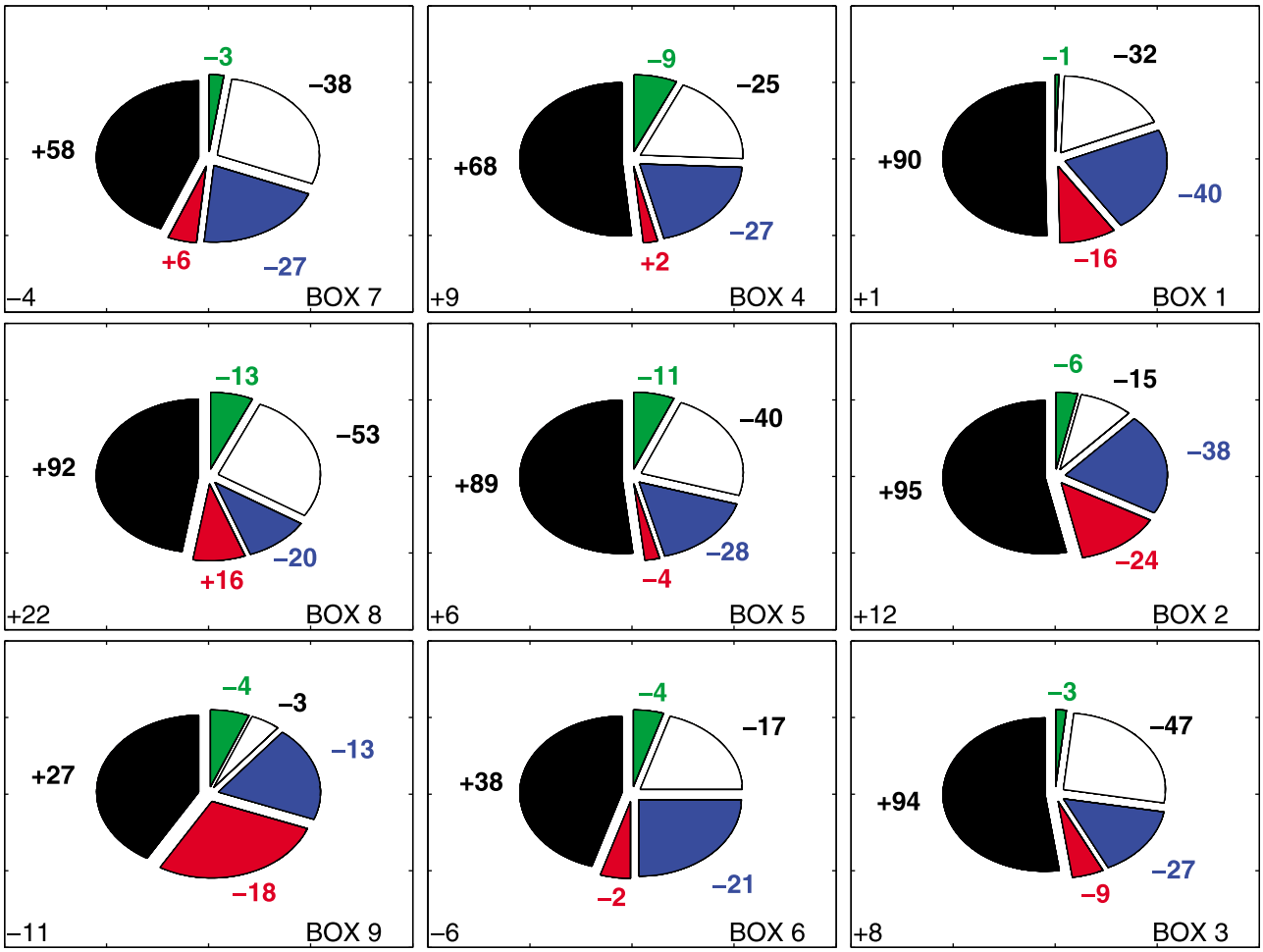

Figure 6. Annual mean of the different terms of equation (7) in the different boxes (in W m^{-2}). The slices represent the percentage of the sum of the absolute values of all the terms on the rhs of equation (7). The net surface heat flux is indicated in black, the entrainment is indicated in green, the residual is indicated in white, the amount of solar radiation passing through the mixed layer base is indicated in blue, and the horizontal advection is indicated in red. The heat storage annual mean is indicated at the lower-left corner of each box.

boxes 8 and 9 are comparable to *Foltz et al.* [2003] at two PIRATA buoys along 10°W (0°N and 6°S) (Figure 8). Both the phase and amplitude of the heat storage are in agreement, despite the differences of data series (see above).

[49] Strong differences exist from box to box. The duration and amplitude of the cooling are larger in the southern boxes 6 and 9 than in the ACT (boxes 2, 5, and 8) despite the fact that the lowest SSTs occur in the ACT. This is due to the fact that the budgets are estimated over the whole MLDs, which are much weaker along and near the equator than southward (Figure 5). The seasonal durations of the cooling range from 3 to 5 months, with minimum duration in the ACT band and maximum duration in the southern boxes.

[50] The seasonal cycles of the different terms on the rhs of equation (7) are presented in Figure 9. The net surface heat flux, the most important contributor to the mixed layer heat budget, exhibits a strong seasonal variability in all boxes, which mainly reflects the seasonality of the heat storage term. Note that, in the southern boxes, the net surface heat fluxes contribute to cool the mixed layer from April to August (a period during which the latent heat fluxes dominate the surface heat budget), while, in the northern boxes, the net surface heat fluxes are positive throughout the year, indicating that solar heat fluxes dominate there.

[51] The amount of short-wave radiation penetrating through the base of the mixed layer (Q_{pen}) does not exhibit a clear seasonal cycle, although higher cooling values are observed in the ACT boxes in late spring and summer, when the MLDs are the weakest. On the contrary, horizontal heat advection shows a clear seasonality in the northern boxes. This seasonality can be put in relation with the Guinea Current (GC). This eastward flowing current is considered as an extension of the North Equatorial Countercurrent (NECC) in boreal summer [*Richardson and Walsh*, 1986; *Arnault*, 1987]. The GC exhibits a minimum (maximum) intensity in boreal winter (summer) and its effect is to warm box 7 in summer, while further east (box 1) cooling occurs from June to December. No seasonality of horizontal heat advection can be clearly detected in the ACT.

[52] Unlike earlier studies showing that upwelling is the main cause of the ACT formation in spring and early summer [e.g., *Weingartner and Weisberg*, 1991], our study

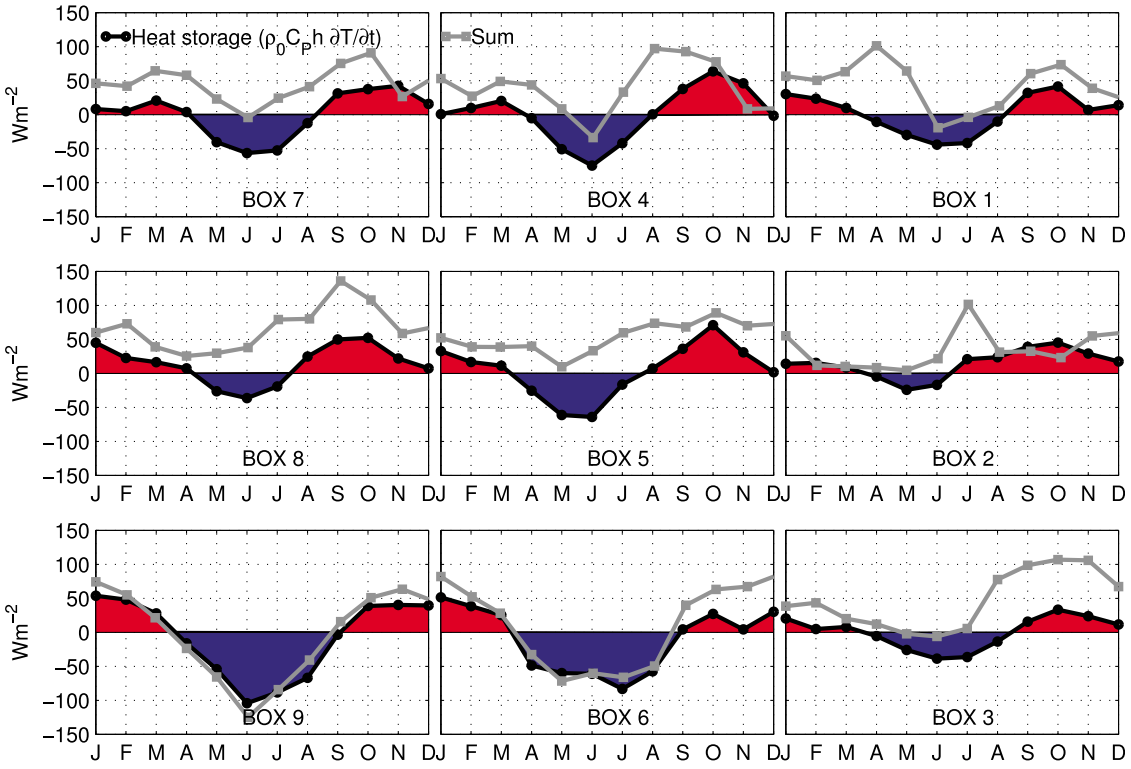

Figure 7. Seasonal cycle of the mixed layer heat storage rate (black) and the sum (gray) of the different terms on the right-hand side of equation (7) for each box, except the residual. Units are W m^{-2}. Red (blue) areas indicate warming (cooling).

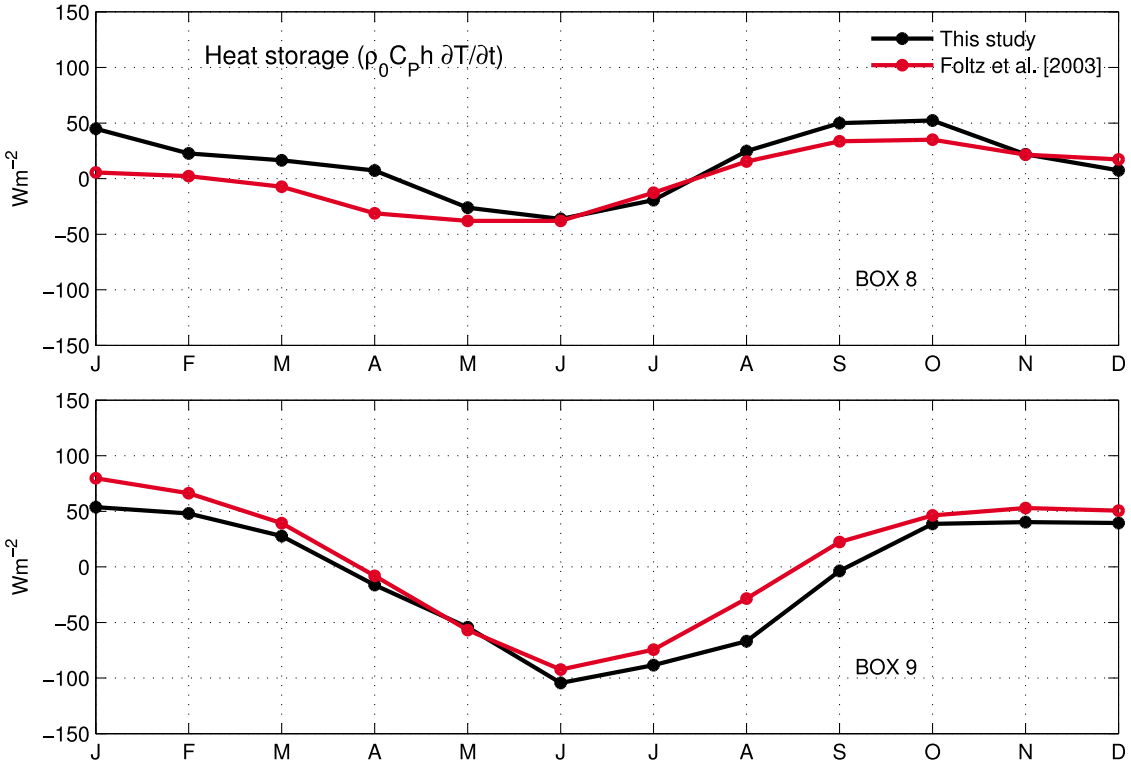

Figure 8. Comparison of the seasonal cycle of heat storage in boxes (top) 8 and (bottom) 9 (black curves) with *Foltz et al.* [2003] at two PIRATA mooring buoys along 10°W at the equator (Figure 8, top) and 6°S (Figure 8, bottom) (red curves).

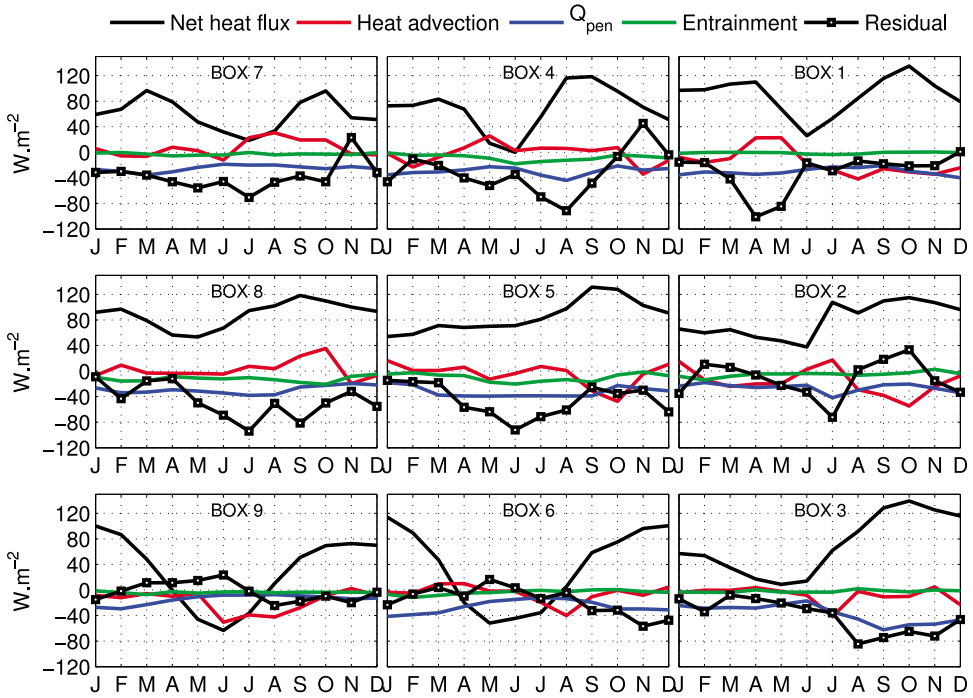

Figure 9. Seasonal cycle of the different terms on the right-hand side of equation (7) in the various boxes. Units are W m^{-2}. The net surface heat flux is indicated in black, the entrainment is indicated in green, the amount of solar radiation passing through the mixed layer base is indicated in blue, and the horizontal advection is indicated in red. The residual is the black curve with squares.

shows a relatively weak contribution of entrainment to the mixed layer heat budget (Figure 9), the seasonal cycle of which is presented in Figure 10. The maximum cooling due to entrainment does not exceed −20 W m^{-2} in all boxes and has the same magnitude as was found by *Foltz et al.* [2003]. Entrainment shows a weak seasonality in the ACT (box 5) and north of the equator (box 4) with maximum cooling in boreal summer.

[53] Recently, *Rhein et al.* [2010], using helium data sampled during EGEE cruises in the EEA in September 2005 and June–July 2006, reported that 48% of the upwelling velocities were smaller than 1.10^{-5} m s^{-1}, 19% were between 1 and 2 10^{-5} m s^{-1}, 22% between 2 and 4 10^{-5} m s^{-1} and 11% of upwelling velocities exceeded these values. In our study, the mean summer vertical velocity computed in the same region gives 1.2 10^{-5} m s^{-1}, which is of the same magnitude as *Rhein et al.*'s [2010] weakest velocities.

[54] The weak contribution of entrainment to the budget in our study, corroborated by *Foltz et al.*'s [2003] results, and the magnitude of vertical velocity estimates by *Rhein et al.* [2010] suggest that entrainment is not only the leading process for cooling the EEA in boreal spring and summer, although its role is to bring the thermocline close to the surface. Other processes are therefore suspected to contribute to the summer cooling.

4.3.3. Significance of the Residual Term at Seasonal Time Scale

[55] In Figure 7, the sum of all the terms on the rhs of equation (7) is nearly always higher than the heat storage term, suggesting that one or several cooling terms are missing in our calculation. The differences between the two curves in Figure 7 are reported in Figure 11, which shows contrasting distribution from box to box, with maximum cooling down to –90 W m^{-2} in the ACT boxes and in the northern boxes, while the residuals are relatively weak in boxes 6 and 9.

[56] The residual includes the errors associated with OSCAR horizontal currents, ECMWF surface heat fluxes, sampling errors and the missing terms (vertical turbulent mixing, horizontal heat diffusion and the temperature and horizontal velocity covariance). Thus, the residual must be carefully interpreted. The errors of each term have been evaluated (Appendix B): this computation indicates that in all boxes entrainment and net surface heat flux errors are the most important in the budget errors. This computation also leads to an error on the residual of the order of 25–30 W m^{-2}, which is less than the amplitude of the residual signal in most boxes. Moreover, in the residual term, vertical turbulent mixing is the only process which is expected to experience a seasonal cycle [e.g., *Foltz et al.*, 2010]. We therefore suspect that the seasonal cycle of the residual is mainly related to the vertical turbulent mixing.

[57] To test this hypothesis, we compared the vertical mixing coefficients at the base of mixed layer (K_v) deduced from the mean June–July–August residuals in each box with independent K_v values reported by *Gouriou and Reverdin* [1992] during the FOCAL/SEQUAL experiments and by *Rhein et al.* [2010] during the EGEE experiment. If we assume that the residuals are only due to vertical mixing,

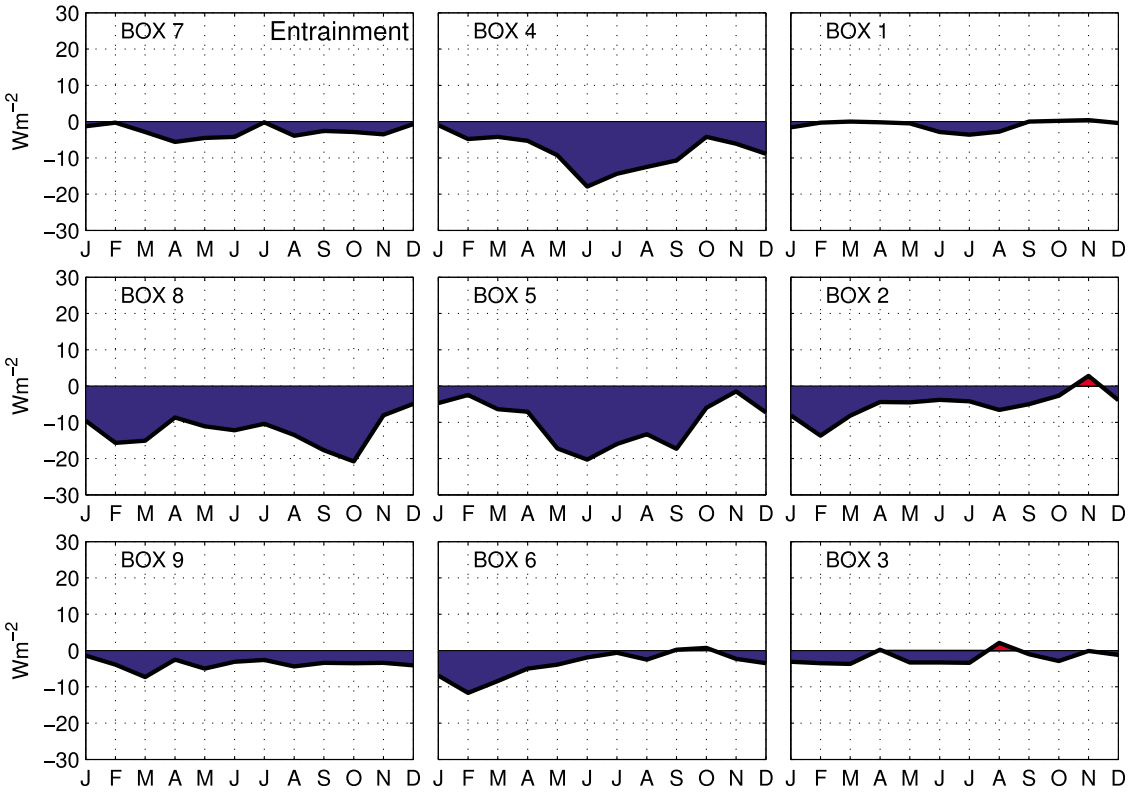

Figure 10. Seasonal cycle of the entrainment term. Blue (red) areas indicate period of cooling (warming).

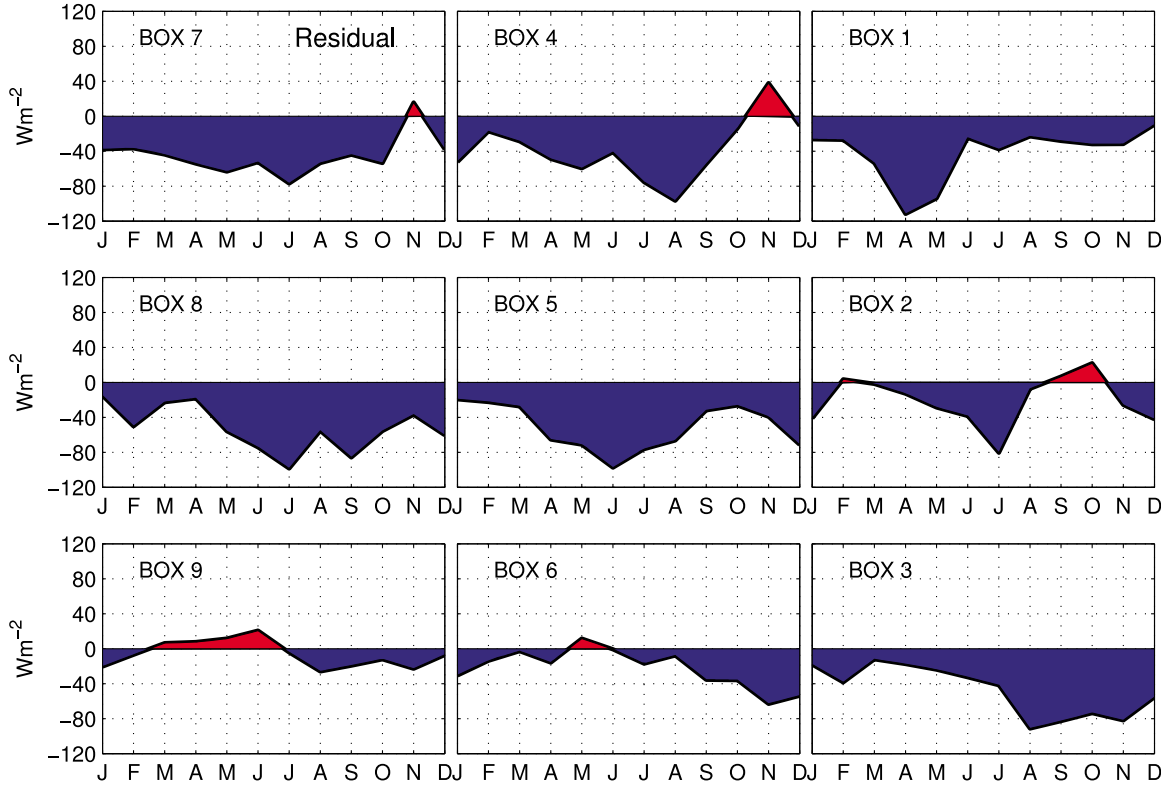

Figure 11. As in Figure 10 but for the residual.

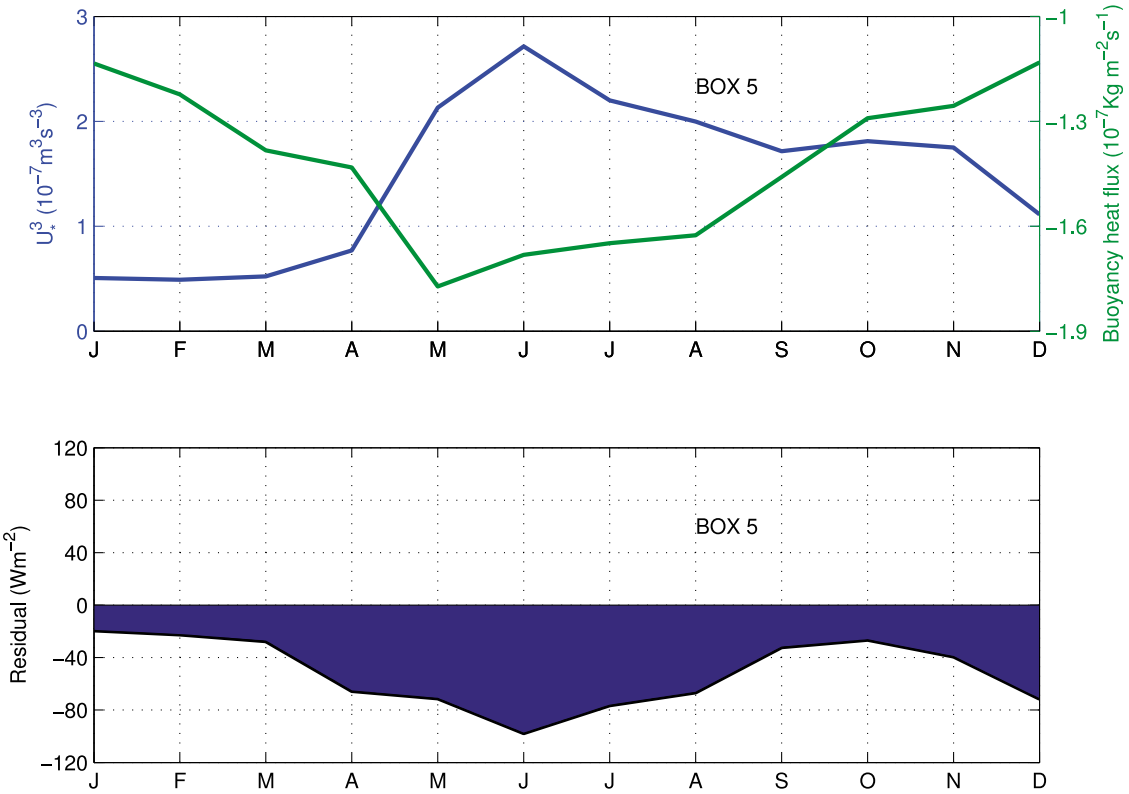

Figure 12. (top) The seasonal cycle of the surface buoyancy flux $B = B_h + B_w$ (green curve) and the cube of the friction velocity $u_*^3 = \left(\frac{\tau}{\rho}\right)^{3/2}$ (blue curve) in box 5 and (bottom) the seasonal cycle of the residual in box 5.

then the mixing coefficients (K_v) can be estimated from the following equation:

$$RES_{JJA} = -\rho_0 C_p K_v \left[\frac{\partial T}{\partial z}\right]_{JJA},$$

where the subscript JJA stands for the period June–July–August. Here the mean vertical gradient $\frac{\partial T}{\partial z}$ is calculated from JJA monthly mean profiles. The values of the mean summer residuals and the associated K_v are reported in Table 1, where they are compared with estimates from *Gouriou and Reverdin* [1992] and *Rhein et al.* [2010]. Mean box values are between 0.3 and 2.0 10^{-4} m^2 s^{-1}, with maxima in the northern boxes (4 and 7) and in the ACT region (boxes 5 and 8) and agree reasonably well with other independent observations. Moreover, high levels of turbulence were reported during the EGEE campaigns in boreal summer (R. Hummels and M. Dengler, personal communication, 2010) associated with diapycnal heat fluxes into the mixed layer down to −60 W m^{-2}, which is also in agreement with values in Table 1.

[58] At a first order, we thus suggest to attribute the residual to the vertical turbulent mixing term, which is known to seriously affect the upper ocean properties, especially in the GG [*Peter et al.*, 2006]. To further examine the causes of the seasonal cycle of the residual and its link with the vertical turbulent mixing, we followed *Foltz et al.* [2010]. At surface, the flux of turbulent kinetic energy provides some additional mixing into the mixed layer. This flux passing from the atmosphere into the mixed layer is a function of the sum of the cube of the friction velocity velocity ($u_*^3 = \left(\frac{\tau}{\rho_0}\right)^{3/2}$, where τ is surface wind stress magnitude and ρ_0 is the density of surface seawater) and the surface buoyancy flux, i.e., $B = B_h + B_w$ (where $B_h = \frac{\alpha}{C_p} Q$ is the component due to the net surface heat flux and $B_w = \beta \rho S(E - P)$ the component due to the freshwater flux. Here, α is the coefficient of thermal expansion of seawater, C_p the heat capacity, Q the net surface heat flux, and β is the coefficient of haline contraction. Evaporation E is calculated as $E = -\frac{H_f}{\rho_0 L_e}$, where H_f is the latent heat flux, L_e the latent heat of vaporization and P the precipitation rate).

[59] The seasonal cycles of the two terms in the ACT (box 5) are reported in Figure 12. The absolute values of the buoyancy forcing and u_*^3 increase strongly in boreal spring and decrease in autumn and winter. In consequence, the vertical turbulent mixing increases in March and reaches a maximum in June. The correlation of the seasonal cycle of the buoyancy forcing and u_*^3 with the seasonal cycle of the residual (0.7 and −0.6, respectively) strengthens the idea that such residual is primarily due to the vertical turbulent mixing. This qualitative analysis provides also a plausible explanation for the observed peak in turbulent mixing during boreal summer.

4.3.4. Interannual Variability

[60] Figure 13 shows the heat storage for the period 2005–2007. The heat storage undergoes strong seasonal cycle each year, with rather similar interannual variability in all boxes except in box 5. In this ACT box, the seasonal cooling took place earlier in 2005 than in 2006 by 1 month:

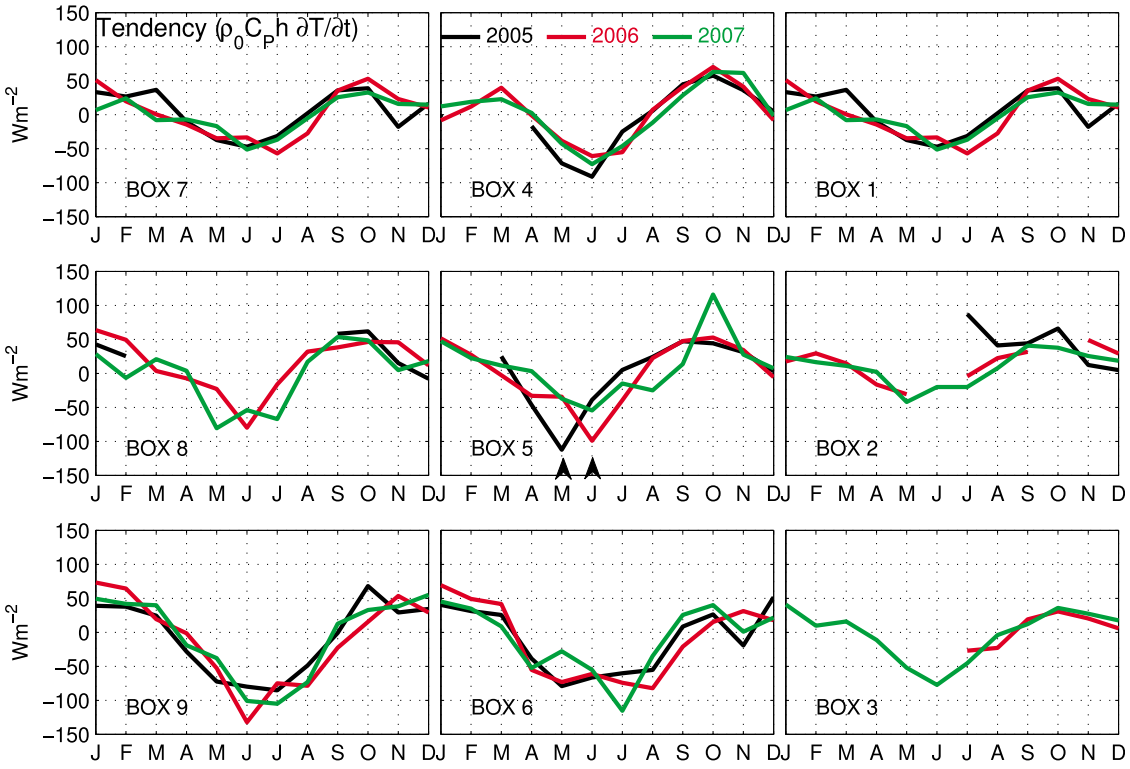

Figure 13. Heat storage rate evolution (W m^{-2}) in the different boxes in 2005 (black), 2006 (red), and 2007 (green).

the same (negative) heat storage minimum was reached (nearly –100 W m^{-2}) in May 2005 and in June 2006. This time shift lasted 3 months, from May to July, after which both heat storages had the same values. The intensity of the cooling was greater during these 2 years compared to 2007, a year during which the ACT was rather warm with a small extended surface area [*Caniaux et al.*, 2011]. A similar evolution was described in the ACT SSTs by *Janicot et al.* [2008] and *Marin et al.* [2009], who also noted that after this time shift of important SST difference (up to 3°C), the maximum cooling was similar in intensity for the 2 years.

[61] Comparing all the terms of the budget in these 3 years showed that the main difference for the setup of the seasonal cooling in May was due to the residual term, which was more negative in 2005 than the other years. This seems to indicate that the turbulent vertical mixing could be the most effective process at that time.

5. Summary and Discussion

[62] In this study, we have investigated the variability of the mixed layer heat content in the eastern equatorial Atlantic by using Argo profiling floats and four PIRATA moored buoys for the period 2005–2007. The formalism proposed by *Caniaux and Planton* [1998] is used to compute the mixed layer heat budget. Almost all the terms of the budget equation can be estimated from Argo data and from various surface reanalysis data sets (ECMWF surface heat fluxes, OSCAR surface currents, and *Reynolds et al.*'s [2007] SSTs). The EEA is subdivided into nine boxes of nearly equal surface area, with respect to the regional dynamical and thermodynamical characteristics, in order to investigate the various mechanisms at play in the EEA.

[63] Besides the quality control (QC) performed by the Coriolis Data Center, we developed additional and more stringent QC procedures, which were applied to the profiles in order to accurately estimate the mixed layer heat budget. In each box, monthly mean SSTs were validated against *Reynolds et al.*'s [2007] SSTs. The two data sets agree reasonably well in terms of amplitude and phase of the SST seasonal cycle with correlations exceeding 90% in all boxes (Figure 4). Both data sets show a clear annual cycle with a maximum in March–April and a minimum in July–August. Subsurface temperatures (Figure 5) also reveal strong interannual variability with stronger cooling in 2005, starting 1 month earlier than in 2006 and 2007, in agreement with EGEE data [*Marin et al.*, 2009]. These results also indicate that the Argo data may be useful for capturing most of the variability in the surface and subsurface temperature field, even in absence of other dedicated in situ platforms (i.e., research cruises, mooring arrays, hydrological surveys, etc), and thus demonstrate the potential importance of using Argo floats to monitor changes in the ocean properties.

[64] On the other hand, the various terms of the annual mean mixed layer heat budget show that the net surface heat flux dominates at all locations and that the amount of shortwave radiation penetrating through the base of the mixed layer contributes to the budget (Figure 6). Heat advection also plays a role in the budget especially in boxes 1, 2 and 9 (see Figure 2 for location) which is associated to the strong system of currents in these regions (termination of the Guinea Current and South Equatorial Undercurrent in the

Table B1. Mean Errors on the Different Terms of the Budget (Equation (7)) Estimated in the Area[a]

Term	Mean Error (W m^{-2})
Heat storage	5.2
Advection	5.2
Entrainment	18.4
Net heat flux	16.6
Amount of solar radiation passing through the mixed layer base	6.5
Residual	26.7

[a]Residual errors were estimated as the square root of the sum of each other squared terms.

two first boxes; South Equatorial Current for the last one). Entrainment is meaningless to the budget on an annual time scale.

[65] The seasonal cycle of heat storage (Figure 7) shows amplitudes ranging from –100 to +75 W m^{-2} with a pronounced minimum in June–July which is associated with the Atlantic cold tongue (ACT) formation south of the equator. It also exhibits a less pronounced, secondary minimum in November–December in boxes north of 4°S (the so-called "little cold season"). The seasonal cycle of each term of the budget shows that the main term that contributes most to the seasonality is the net surface heat flux, which has a strong minimum in summer in the area and a maximum in September–October (Figure 9). The summer minimum is associated with extended cloud cover reducing the downwelling solar radiation in the northern part of the Gulf of Guinea while, in the south, the minimum is associated with intense latent heat fluxes. These results support the idea that, unlike those in the Pacific, where dynamical processes are dominant, Atlantic SSTs are controlled by both thermodynamical and dynamical processes [*Giannini et al.*, 2000; *Seager et al.*, 2000].

[66] The sum of the terms in equation (7) is always greater than the heat storage term, meaning that a cooling term is missing in the mixed layer heat budget (Figure 7). The seasonal cycle of the residual indicates strongest cooling in summer, especially in northern and ACT boxes. The residuals include errors associated to OSCAR horizontal currents, ECMWF surface heat fluxes, sampling errors, and themissing terms (vertical turbulent mixing, horizontal diffusion, and the temperature and horizontal velocity covariance). However, comparison of the residual with independent turbulent mixing data [*Gouriou and Reverdin*, 1992; *Rhein et al.*, 2010] indicated good agreement (Table 1). The residual is therefore thought to be associated, to the first order, with the vertical turbulent mixing. This term experiences strong values in both the northern and the ACT boxes. To confirm this idea, we examined the correlations between the residual and the surface buoyancy forcing and u_*^3. The correlations proved to be high enough to support the hypothesis that most of the residual is due to the vertical mixing. If this hypothesis holds, it means that vertical mixing could be the second most important process of the annual mixed layer heat budget in the region of the ACT (nearly 25%) after the net surface heat fluxes (nearly 50%).

[67] Unexpectedly, the residual in the region north of the equator is nearly as high as in the ACT. Despite the fact that this could be due to errors (associated to surface heat fluxes and to sampling), a possible explanation could be the shear between the surface eastward Guinea Current and the subsurface westward Guinea Undercurrent [e.g., *Lemasson and Rebert*, 1968], a current (identified by these authors as the "Ivorian Undercurrent") which flows westward, opposite to the Guinea Current. Moreover shelf processes could also contribute to enhance vertical mixing in the northern boxes. It would be very interesting to verify whether the importance of this process is confirmed by similar budgets in realistic numerical models [*Jouanno et al.*, 2011].

Appendix A: Quality Control

[68] The quality control procedure used in this study for both the Argo and PIRATA data consisted of the following steps:

[69] 1. We first eliminate missing readings from the profiles.

[70] 2. We then linearly interpolate profiles every 1 m depth. If the first observation value is not at the surface, extrapolate it to the surface and refer to it as SST. The profiles show that the sampling depths were not uniform and most of the profiles consisted of about 120 levels from the surface to 2000 m depth.

[71] 3. To check whether the extrapolated SSTs are consistent and lie within seasonal SST values, we compare them with the daily *Reynolds et al.* [2007] SSTs interpolated along the float trajectory. This range is defined as follows: extrapolated SSTs which are more than 2°C below the Reynolds SSTs are removed from the time series. Visual inspections of those profiles show that the first observed temperature levels are so deep that the extrapolation of those temperatures to the surface leads to cooler SSTs than the Reynolds' SSTs. This means that extrapolating temperatures in the thermocline to the surface leads to discrepancies up to 4°C. This is especially true in the Gulf of Guinea, where the mixed layer depths are very small (less than 30 m).

[72] 4. Finally, we also exclude profiles with density inversion and spikes.

[73] Our quality control check removed 7% of all Argo profiles and 5% of PIRATA profiles.

Appendix B: Error Estimates

[74] We estimated the errors on each term of the budget, by applying the same procedure as *Foltz and McPhaden* [2009] and by evaluating the mean annual values of the atmospheric and oceanic parameters in each box. The errors do not vary much throughout the different boxes and the domain average errors are given in the following Table B1. The errors on the net surface heat flux are comparable to the differences obtained when comparing fluxes from different NWP models.

[75] **Acknowledgments.** This study was supported by the AMMA project. Based on a French initiative, AMMA was built by an international scientific group and is currently funded by a large number of agencies, including those in France, the United Kingdom, the United States, and Africa. It has been the beneficiary of a major financial contribution from the European Community's Sixth Framework Research Programme. Detailed information on scientific coordination and funding is available on the AMMA International Web site http://www.amma-international.org. Special thanks are due to Elodie Kestenare and Christine Coatanoan who helped in the quality control of Argo data set provided by Coriolis Data Center at the French Institute for Exploitation of the Sea (IFREMER). We acknowledge the PIRATA Project and TAO Project Office at NOAA/

PMEL for providing open access to PIRATA data. We warmly thank Gregory Foltz who provided us his mixed layer budget time series and routines for calculating errors in different terms in our mixed layer heat budget. Finally, we also thank three anonymous reviewers for their useful comments on the manuscript.

References

Arnault, S. (1987), Tropical Atlantic geostrophic currents and ship drifts, *J. Geophys. Res.*, *92*, 5076–5088, doi:10.1029/JC092iC05p05076.

Bakun, A. (1978), Guinea Current upwelling, *Nature*, *271*, 147–150, doi:10.1038/271147a0.

Bonjean, F., and G. S. E. Lagerloef (2002), Diagnostic model and analysis of the surface currents in the tropical Pacific Ocean, *J. Phys. Oceanogr.*, *32*, 2938–2954, doi:10.1175/1520-0485(2002)032<2938:DMAAOT>2.0.CO;2.

Bourlès, B., P. Brandt, G. Caniaux, M. Dengler, Y. Gouriou, E. Key, R. Lumpkin, F. Marin, R. L. Molinari, and C. Schmid (2007), African Monsoon Multidisciplinary Analysis (AMMA): Special measurements in the Tropical Atlantic, *CLIVAR Newsl. Exch.*, *41*(12), 7–9.

Bourlès, B., et al. (2008), The PIRATA program: History and accomplishments of the 10 first years tropical Atlantic observing system's backbone, *Bull. Am. Meteorol. Soc.*, *89*, 1111–1125, doi:10.1175/2008BAMS2462.1.

Brandt, P., G. Caniaux, B. Bourlès, A. Lazar, M. Dengler, A. Funk, V. Hormann, H. Giordani, and F. Marin (2011), Equatorial upper-ocean dynamics and their interaction with the West African monsoon, *Atmos. Sci. Lett.*, *12*, 24–30, doi:10.1002/asl.287.

Caniaux, G., and S. Planton (1998), A three-dimensional ocean mesoscale simulation using data from the SEMAPHORE experiment: Mixed layer heat budget, *J. Geophys. Res.*, *103*, 25,081–25,099, doi:10.1029/98JC00452.

Caniaux, G., F. Guichard, D. Bourras, E. Key, H. Giordani, and B. Bourlès (2007), Evaluation of sea surface flux fields from NWP models, paper presented at Second AMMA International Conference, Karlsruhe, Germany, 26–30 Nov.

Caniaux, G., H. Giordani, J.-L. Redelsperger, F. Guichard, E. Key, and M. Wade (2011), Couplings between the Atlantic cold tongue, the St Helena anticyclone, and the African monsoon in boreal spring and summer, *J. Geophys. Res.*, *116*, C04003, doi:10.1029/2010JC006570.

Carton, J. A., and Z. X. Zhou (1997), Annual cycle of sea surface temperature in the tropical Atlantic Ocean, *J. Geophys. Res.*, *102*, 27,813–27,824, doi:10.1029/97JC02197.

Colin, C. (1988), Coastal upwelling events in front of Ivory Coast during the FOCAL program, *Oceanol. Acta*, *11*, 125–138.

de Boisséson, E., V. Thierry, H. Mercier, and G. Caniaux (2010), Subpolar mode water formation in the Iceland basin: Mixed layer heat budgets, *J. Geophys. Res.*, *115*, C10055, doi:10.1029/2010JC006283.

de Boyer Montégut, C., G. Madec, A. S. Fischer, A. Lazar, and D. Iudicone (2004), A global mixed layer depth climatology based on individual profiles, *J. Geophys. Res.*, *109*, C12003, doi:10.1029/2004JC002378.

de Coëtlogon, G., S. Janicot and A. Lazar (2010), Intraseasonal variability of the ocean-atmosphere coupling in the Gulf of Guinea during boreal spring and summer, *Q. J. Roy. Meteorol. Soc.*, 426–441, doi:10.1002/qj.554.

Foltz, G. R., and M. J. McPhaden (2009), Impact of the bayer layer thickness on SST in the central tropical North Atlantic, *J. Clim.*, *22*, 285–299, doi:10.1175/2008JCLI2308.1.

Foltz, G. R., S. A. Grodsky, J. A. Carton, and M. J. McPhaden (2003), Seasonal mixed layer heat budget of the tropical Atlantic Ocean, *J. Geophys. Res.*, *108*(C5), 3146, doi:10.1029/2002JC001584.

Foltz, G. R., J. A. Carton, and E. P. Chassignet (2004), Tropical instability vortices in the Atlantic Ocean, *J. Geophys. Res.*, *109*, C03029, doi:10.1029/2003JC001942.

Foltz, G. R., J. Vialard, P. Kumar, and M. J. McPhaden (2010), Seasonal mixed layer heat balance of the southwestern tropical Indian Ocean, *J. Clim.*, *23*, 947–965, doi:10.1175/2009JCLI3268.1.

Giannini, A., Y. Kushnir, and M. A. Cane (2000), Interannual variability of Caribbean rainfall, ENSO, and the Atlantic Ocean, *J. Clim.*, *13*, 297–311, doi:10.1175/1520-0442(2000)013<0297:IVOCRE>2.0.CO;2.

Gould, W. J. (2005), From Swallow floats to Argo—The development of neutrally buoyant floats, *Deep Sea Res. Part II*, *52*, 529–543, doi:10.1016/j.dsr2.2004.12.005.

Gouriou, Y., and G. Reverdin (1992), Isopycnal and diapycnal circulation of the upper equatorial Atlantic Ocean in 1983–1984, *J. Geophys. Res.*, *97*, 3543–3572, doi:10.1029/91JC02935.

Gu, G., and R. F. Adler (2004), Seasonal evolution and variability associated with the West African monsoon system, *J. Clim.*, *17*, 3364–3377, doi:10.1175/1520-0442(2004)017<3364:SEAVAW>2.0.CO;2.

Hadfield, R. E., N. C. Wells, S. A. Josey, and J. J. M. Hirschi (2007), On the accuracy of North Atlantic temperature and heat storage fields from Argo, *J. Geophys. Res.*, *112*, C01009, doi:10.1029/2006JC003825.

Helber, R. W., R. H. Weisberg, F. Bonjean, E. S. Johnson, and G. S. E. Lagerloef (2007), Satellite-derived surface current divergence in relation to tropical Atlantic SST and wind, *J. Phys. Oceanogr.*, *37*, 1357–1375, doi:10.1175/JPO3052.1.

Hormann, V., and P. Brandt (2007), Atlantic Equatorial Undercurrent and associated cold tongue variability, *J. Geophys. Res.*, *112*, C06017, doi:10.1029/2006JC003931.

Janicot, S., et al. (2008), Large-scale overview of the summer monsoon over West and central Africa during AMMA field experiment in 2006, *Ann. Geophys.*, *26*, 2569–2595, doi:10.5194/angeo-26-2569-2008.

Jochum, M., and R. Murtugudde (2006), Temperature advection by tropical instability waves, *J. Phys. Oceanogr.*, *36*, 592–605, doi:10.1175/JPO2870.1.

Johnson, E. S., F. Bonjean, G. S. E. Lagerloef, J. T. Gunn, and G. T. Mitchum (2007), Validation and error analysis of OSCAR sea surface currents, *J. Atmos. Oceanic Technol.*, *24*, 688–701, doi:10.1175/JTECH1971.1.

Jouanno, J., M. Marin, Y. du Penhoat, J. M. Moline, and J. Sheinbaum (2011), Seasonal modes of surface cooling in the Gulf of Guinea, *J. Phys. Oceanogr.*, doi:10.1175/JPO-D-11-031.1, in press.

Lamb, P. J. (1978), Large-scale tropical Atlantic surface circulation patterns associated with sub-Saharan weather anomalies, *Tellus*, *30*, 240–251, doi:10.1111/j.2153-3490.1978.tb00839.x.

Lemasson, L., and J.-P. Rebert (1968), Observations de courants sur le plateau continental ivoirien: Mise en évidence d'un sous-courant, *Doc. Sci. Prov. Cent. Rech. Oceanogr. Abidjan*, *22*, 1–66CRO Abidjan.

Marin, F., G. Caniaux, B. Bourlès, H. Giordani, Y. Gouriou, and E. Key (2009), Why were sea surface temperatures so different in the eastern equatorial Atlantic in June 2005 and 2006?, *J. Phys. Oceanogr.*, *39*, 1416–1431, doi:10.1175/2008JPO4030.1.

Menkes, C. E. R., J. G. Vialard, S. C. Kennan, J. P. Boulanger, and G. V. Madec (2006), A modeling study of the impact of tropical instability waves on the heat budget of the eastern equatorial Pacific, *J. Phys. Oceanogr.*, *36*, 847–865, doi:10.1175/JPO2904.1.

Merle, J. (1980), Seasonal heat budget in the equatorial Atlantic Ocean, *J. Phys. Oceanogr.*, *10*, 464–469, doi:10.1175/1520-0485(1980)010<0464:SHBITE>2.0.CO;2.

Ohlmann, J. C. (2003), Ocean radiant heating in climate models, *J. Clim.*, *16*, 1337–1351, doi:10.1175/1520-0442-16.9.1337.

Ohno, Y., T. Kobayashi, N. Iwasaka, and T. Suga (2004), The mixed layer depth in the North Pacific as detected by the Argo floats, *Geophys. Res. Lett.*, *31*, L11306, doi:10.1029/2004GL019576.

Peter, A. C., M. Le Hénaff, Y. du Penhoat, C. E. Menkes, F. Marin, J. Vialard, G. Caniaux, and A. Lazar (2006), A model study of the seasonal mixed layer heat budget in the equatorial Atlantic, *J. Geophys. Res.*, *111*, C06014, doi:10.1029/2005JC003157.

Philander, S. G. H., and R. C. Pacanowski (1986), A model of the seasonal cycle in the tropical Atlantic Ocean, *J. Geophys. Res.*, *91*, 14,192–14,206, doi:10.1029/JC091iC12p14192.

Picaut, J. (1983), Propagation of the seasonal upwelling in the eastern equatorial Atlantic, *J. Phys. Oceanogr.*, *13*, 18–37, doi:10.1175/1520-0485(1983)013<0018:POTSUI>2.0.CO;2.

Redelsperger, J.-L., C. Thorncroft, A. Diedhiou, T. Lebel, D. Parker, and J. Polcher (2006), African Monsoon Multidisciplinary Analysis: An international project and field campaign, *Bull. Am. Meteorol. Soc.*, *87*, 1739–1746, doi:10.1175/BAMS-87-12-1739.

Reynolds, R. W., T. M. Smith, C. Liu, D. B. Chelton, K. S. Casey, and M. G. Schlax (2007), Daily high-resolution blended analyses for sea surface temperature, *J. Clim.*, *20*, 5473–5496, doi:10.1175/2007JCLI1824.1.

Rhein, M., M. Dengler, J. Sültenfuß, R. Hummels, S. Hüttl-Kabus, and B. Bourlès (2010), Upwelling and associated heat flux in the equatorial Atlantic inferred from helium isotope disequilibrium, *J. Geophys. Res.*, *115*, C08021, doi:10.1029/2009JC005772.

Richardson, P. L., and S. G. H. Philander (1987), The seasonal variations of surface currents in the tropical Atlantic Ocean: A comparison of ship drift data with results from a general circulation model, *J. Geophys. Res.*, *92*, 715–724, doi:10.1029/JC092iC01p00715.

Richardson, P. L., and D. Walsh (1986), Mapping climatological seasonal variations of surface currents in the tropical Atlantic using ship drifts, *J. Geophys. Res.*, *91*, 10,537–10,550, doi:10.1029/JC091iC09p10537.

Riser, S. (2009), A review of recent problems with CTD units and Druck pressure sensors, *Argo Newsl.*, *11*, 2–3.

Roemmich, D., et al. (2001), Argo: The global array of profiling floats, in *Observing the Ocean in the 21st Century*, edited by C. J. Koblinsky and N. R. Smith, pp. 248–258, Global Ocean Ddat Assimilation Exp. Proj. Off. Bur. of Meteorol, Melbourne, Australia.

Seager, R., Y. Kushnir, M. Visbeck, N. Naik, J. Miller, G. Krahmann, and H. Cullen (2000), Causes of Atlantic Ocean climate variability between 1958 and 1998, *J. Clim.*, *13*, 2845–2862, doi:10.1175/1520-0442(2000)013<2845:COAOCV>2.0.CO;2.

Stramma, L., and F. Schott (1999), The mean flow field of the tropical Atlantic Ocean, *Deep Sea Res. Part II*, *46*, 279–303, doi:10.1016/S0967-0645(98)00109-X.

Sweeney, C., A. Gnanadesikan, S. M. Griffies, M. J. Harrison, A. J. Rosati, and B. L. Samuel (2005), Impacts of shortwave penetration depth on large-scale ocean circulation and heat transport, *J. Phys. Oceanogr.*, *35*, 1103–1119, doi:10.1175/JPO2740.1.

Swenson, M. S., and D. V. Hansen (1999), Tropical Pacific ocean mixed layer heat budget: The Pacific cold tongue, *J. Phys. Oceanogr.*, *29*, 69–81, doi:10.1175/1520-0485(1999)029<0069:TPOMLH>2.0.CO;2.

Vauclair, F., and Y. du Penhoat (2001), Interannual variability of the upper layer of the tropical Atlantic Ocean from in situ data between 1979 and 1999, *Clim. Dyn.*, *17*, 527–546, doi:10.1007/s003820000125.

Wang, W., and M. J. McPhaden (1999), The surface layer heat balance in the equatorial Pacific ocean. Part I: Mean seasonal cycle, *J. Phys. Oceanogr.*, *29*, 1812–1831, doi:10.1175/1520-0485(1999)029<1812:TSLHBI>2.0.CO;2.

Weingartner, T. J., and R. H. Weisberg (1991), On the annual cycle of equatorial upwelling in the central Atlantic Ocean, *J. Phys. Oceanogr.*, *21*, 68–82, doi:10.1175/1520-0485(1991)021<0068:OTACOE>2.0.CO;2.

Wells, N. C., S. A. Josey, and R. E. Hadfield (2009), Towards closure of regional heat budget in the North Atlantic using Argo floats and surface flux datasets, *Ocean Sci.*, *5*, 59–72, doi:10.5194/os-5-59-2009.

Yu, L., X. Jin, and R. A. Weller (2006), Role of net surface heat flux in seasonal variations of sea surface temperature in the tropical Atlantic Ocean, *J. Clim.*, *19*, 6153–6169, doi:10.1175/JCLI3970.1.

G. Caniaux, CNRM/GAME, Météo-France/CNRS, 42 Av. Gustave Coriolis, F-31057 Toulouse, France.

Y. du Penhoat, LEGOS, IRD, LEGOS, 14 Av. Edouard Belin, F-31400 Toulouse, France.

M. Wade, LPAOSF, UCAD, BP 5085, Dakar, Senegal. (malick172@yahoo.fr)